Interaction among Local Flows, UHI, Coastal Winds, and Complex Terrain: Effect on Urban-scale Temperature and Building Energy Consumption during Heatwaves

Ruiqing Du [a], Chun-Ho Liu [a, *], Xianxiang Li [b, c, d], Chuan-Yao Lin [e]

[a] *Department of Mechanical Engineering, The University of Hong Kong, Hong Kong*
[b] *School of Atmospheric Sciences, Sun Yat-sen University, China*
[c] *Key Laboratory of Tropical Atmosphere-Ocean System, Ministry of Education, China*
[d] *Southern Marine Science and Engineering Guangdong Laboratory (Zhuhai), China*
[e] *Research Center for Environmental Changes, Academia Sinica, Taipei, Taiwan*

Revised Manuscript **No. ENB-D-23-02853**
submitted
to
Energy and Buildings
on
November 3, 2023

**Correspondence:*
Chun-Ho LIU
Department of Mechanical Engineering,
7/F Haking Wong Building,
The University of Hong Kong,
Pokfulam Road, Hong Kong SAR, CHINA

Tel: +852 3917 7901 / + 852 9788 7951
Fax: +852 2858 5415
liuchunho@graduate.hku.hk
https://aplhk.tech
ORCID: 0000-0002-4609-524X

Abstract

Extreme heat aggravates thermal stress and electricity shortage in urban areas. This study investigates the (circulating) winds in Hong Kong during a heatwave. Unprecedentedly, the collective effect of coastal winds, complex terrain, and local flows on urban temperatures and air-conditioning load intensity (ACLI) is examined using the mesoscale Weather Research and Forecasting (WRF) model. Three representative wind patterns, including urban-accelerated channel wind, channel-wind-induced heat advection, and urban-mountain-stagnated sea-breeze, are analyzed. Our results show that the mountain blockage in foothill areas would increase 2-m temperatures ($T2$) and ACLI by 1 °C to 2 °C and 5 W m^{-2}, respectively. ACLI in compact high-rise areas (LCZ 1) is most sensitive to extreme heat. Moreover, the urban heat island (UHI) downstream is crucial that would accelerate channel flows by 1.66 m sec^{-1} (50.26 %). On the other hand, terrain-induced channel winds augment heat advection, increasing downstream $T2$ (0.7 °C) and ACLI (2.62 W m^{-2}). UHI-induced local flows interact with hilly slopes, stagnating the sea breeze on mountain leeward side. Subsequently, the winds would be slowed down by 0.81 m sec^{-1} while the temperature $T2$ would be increased by 0.9 °C in downstream urban areas. Eventually, the daytime ACLI could be raised as much as 6.41 W m^{-2}.

(200 words)

Keywords: air-conditioning (AC) load; building category (BC); building energy consumption; coastal effect; complex terrain; energy policy; local climate zone (LCZ); local flows; sustainable strategy development; Weather Research and Forecasting (WRF) model.

1. Introduction

Rapid urbanization has altered notably urban microclimate. Some phenomena, such as urban heat island (UHI), where urban temperatures are higher than those of the surrounding (rural) areas, have attracted increasing attention. The extreme warmth could pose a threat to public health, energy consumption, and infrastructure security, especially during heatwave events. One of the challenges is surging air-conditioning (AC) load for space cooling. During summer time, the AC-related electricity demand in China and the United States could exceed 50% of the total [1, 2] that could even paralyze the power grid [3]. Therefore, unraveling the UHI mechanism and its effect on city-scale AC load intensity (ACLI) is crucial to tackle the heat-related risk.

UHI intensities (UHIIs) not only depend on the city characteristics but also the surrounding landuse/landcover (LULC) and topography [4, 5]. Inhomogeneous LULC and terrain might induce buoyant flows by creating temperature gradients between: (i) sea and land (sea/land breeze), (ii) urban and rural areas (UHI breeze), (iii) LULC of various radiative properties (micro-circulation), together with (iv) slopes, valleys, and adjacent planes (mountain-valley flows) [6]. Besides, the channeling and blocking caused by mountains and urban canyons modify local flows [7, 8]. These local winds in turn alter substantially the temperatures and transport in urban areas, creating microclimate of different scales [5]. When a city is situated within coastal areas adjacent to complex terrain, UHI circulation, sea-land breeze, and mountain-valley circulation coexist, further complicating urban microclimate [5, 6]. The existing high-resolution (800 m) convection-permitting simulation over Sydney found that Foehn wind (sea breeze) could increase (decrease) the UHII by 10.17 °C (11.43 °C) [5]. Besides, local flows extended UHI coverage beyond city boundary by heat advection. Urban heat advection was also found significant in Birmingham, augmenting air temperature by 1.9 °C [9]. In addition, it was reported that sea breeze combines with upslope wind that could change the wind-flow structure under mild synoptic conditions in Taiwan [10]. Moreover, the topography in Sao Paulo was found to enhance sea breeze propagation that intensified urban-rural-temperature gap by 2 °C [11]. Thus, it is important to study the influence of local winds on UHII and the physical implication behind, in particular for coastal cities.

Local flows would also affect city-scale AC load by modifying temperatures and winds. An extensive data analysis found that the building energy consumption in poorly ventilated urban areas could be increased by 6.704% [12]. During extreme temperature events, this change in temperature could be fatal for power grids which are already on the verge of collapse due to surging loads [3]. On the other hand, coastal dynamics, such as sea breeze, considerably reduced the AC energy demand by around 15 W m^{-2} in New York [13]. Hence, the pressing need for a thorough understanding of the effect of local winds on city-scale building energy consumption arises.

Urban energy engineers have coupled microclimate models, such as computational fluid dynamics (CFD) with building energy models (BEMs) to solve the local winds within urban canopy layer and their effects on AC load [14]. These models simulate weather data and thermo-radiative processes at refined scales. Their scales are mostly limited in small urban areas but the computation is expensive. In contrast, climatologists have developed mesoscale models with urban canopy models that are able to handle synoptic conditions and mesoscale meteorological processes. The computational costs are lessened, realizing larger city-scale modeling [14, 15].

Weather Research and Forecasting (WRF) model couples the Building Effect Parameterization (BEP) and Building Energy Model (BEM) that is a promising solution to urban-scale climate and AC load prediction [16]. WRF encompasses natural terrain, real weather conditions, as well as mesoscale meteorological processes in simulation. Apart from climate change [17, 18] and local microclimate [19], existing studies have widely used WRF to quantify the benefit of UHI mitigation strategies, such as high-albedo surfaces [20, 21], photovoltaic panels [22, 23], and passive cooling techniques [24], in terms of building energy. These efforts demonstrated the importance of mesoscale meteorological processes to urban-scale building energy consumption. Besides, it enables the modeling of microclimate and AC load at large city scale. As such, the interaction among city zones, such as heat exchange due to local winds, could be well represented.

BEP/BEM [25, 26] simplifies urban morphology in the form of infinitely long streets with uniform width but different building geometry. It assigns the building dimensions, street-canyon aspect ratios, building height distributions, surface albedo, and material thermal properties, etc., according to LULC. The model calculates separately the surface-energy budget for streets, roofs, and facades to estimate the sensible heat exchange between buildings and the atmosphere. The influence of shading and trapping in street canyons for radiation calculations is also included. This simplification enables an efficient computation in mesoscale modeling. BEM calculates the two-way energy exchange and the anthropogenic heat (AH) based on weather conditions. It considers the advective, conductive, and radiative heat transfer between indoor and outdoor space, walls and floors, together with heating, ventilation, and air conditioning (HVAC).

WRF-BEP/BEM has been used to assess urban-scale energy consumption elsewhere [27]. Most of the existing studies have used the LULC data to define the urban morphology and building categories in three classes: commercial or industrial, high intensity residential, and low intensity residential. Recently, the Local Climate Zone (LCZ) was extensively mapped in the World Urban Database Access Portal Tools (WUDAPT) project [28]. It has a more detailed classification, consisting of 10 classes for built areas. However, the LCZ cannot include building category that weakens its functionality of BEM. Compared with chaining strategies, WRF-BEP/BEM uses coupling to integrate the feedback from BEM, such as anthropogenic heat, to urban climate modeling. Moreover, it handles well the dynamical interaction between local wind and building energy consumption. In contrast, chaining strategies simulate the climate output by WRF first which is then input into BEM [29]. This approach enables the detailed modeling of building characteristics at the expense of ignoring the two-way interaction between the buildings and the neighborhood context. Besides, WRF-BEP/BEM was improved recently, enhancing its modeling accuracy as well as functionality [30, 31].

In this study, we investigate how topography, land-sea breeze, and UHI breeze synergistically affect the urban temperatures and AC load in an Asian metropolis, Hong Kong (HK). HK is a typical coastal city with large population (7.41 million [32]) but limited land space (1,064 km^2) in which 70% is hilly terrain. Coastal areas are attractive to human settlement because of the convenient transport, abundant natural resource, as well as ecological benefit [33]. Nowadays, more than half of the world population lives in coastal cities (< 200 km measuring from the coastline). In fact, most people reside in riparian areas with complex terrain [33, 34]. The surrounding maritime surfaces and mountains in HK complicate the wind patterns. Besides, HK has a compact, high-rise urban setting with subtropical climate where is hot in summer, especially during heatwave events (maximum temperature 35.5 °C). Extreme temperatures would surge the ACLI for space cooling [35]. During the summer in HK, the peaked AC load could jump to 66% of the output [36]. Power companies even have to mitigate power-grid overload by raising electricity tariff [37].

To the best knowledge of the authors, previous studies have examined individual or two types of local flows, such as modification of UHI circulation by land-sea breeze, and vice versa. Whereas, the coupling among UHI, coastal winds, complex terrain, and buoyant flows, remains an open question. For instance, how sea breeze, slope flows, and urban-rural circulation interact, together with their collective influence on UHII and AC load. Moreover, the heat transfer from upwind urban areas is attributed to local flows. The subsequent temperature variation is yet to be quantified. Furthermore, CFD models coupled with BEM were rarely tested for synoptic, mesoscale meteorological processes. Besides, these coupled models focused on individual neighborhood or block scale rather than larger city scale. In this connection, the advective heat transfer among various neighborhood zones is seldom examined by urban-scale BEMs (UBEMs).

To bridge the aforementioned knowledge gap, we integrate the local climate zone (LCZ) defined in the World Urban Database and Access Portal Tools (WUDAPT) and building category (BC) map into the multi-layer WRF model. The coupled WRF-WUDAPT/BC model is applied to calculate the spatio-temporal patterns of UHII and AC load in response to local-flow scenarios during a typical heatwave event in Hong Kong (June 23 to 28, 2016) [38].

In contrast to previous studies, this paper adds new dimensions to the mechanism of urban airflows: the coupling among UHI, land-sea breeze, mountainous topography, and local flows. In addition, the effect of local flows on building energy consumption is examined within a multiscale framework connecting to mesoscale boundaries. Furthermore, the indirect effect of upstream/downstream terrain and heat advection on UHII and ACLI is quantified for the first time. The outcome will provide references for urban thermal comfort and sustainable energy policy.

2. Methodology

2.1 Model Configuration

Advanced WRF (ARW version 3.6.1) [39] is used in this study that consists of four one-way nested domains at 9 km (241×181 grids), 3 km (271×181), 1 km (241×181), and 0.33

km (241×181) spatial resolution (Figure 1). Apart from the refined 10-m resolution in the urban canopy, there are 51 η vertical levels from the ground to 50 hPa for the atmospheric model. The initial and boundary conditions are collected from European Centre for Medium-Range Weather Forecasts (ECMWF) ERA-Interim datasets at 6-hour and 0.75° intervals. Specifically, to study the UHI mechanism in summer, a 160-hour WRF calculation (from 0800 LST on June 21, 2016 to 2300 LST on June 27, 2016) is conducted. After the first 40 hours of spin-up (0800 LST on June 21, 2016 to 2300 LST on June 22, 2016), a typical 120-hour heatwave event (0000 LST on June 23, 2016 to 2300 LST on June 27, 2016) [40] is selected as the analysis period. During that heatwave event as defined by the Hong Kong Observatory (HKO) [40, 41], the monthly-average maximum temperature hit a record high of 32.4 ºC. Besides, the daily maximum temperatures were above 35 °C for four consecutive days (from June 24 to 27, 2016), breaking the weather record of three consecutive days (from May 30 to June 1, 1963). In particular, the maximum hourly temperature was recorded as hot as 35.5 °C at 1400 LST on June 25, 2016.

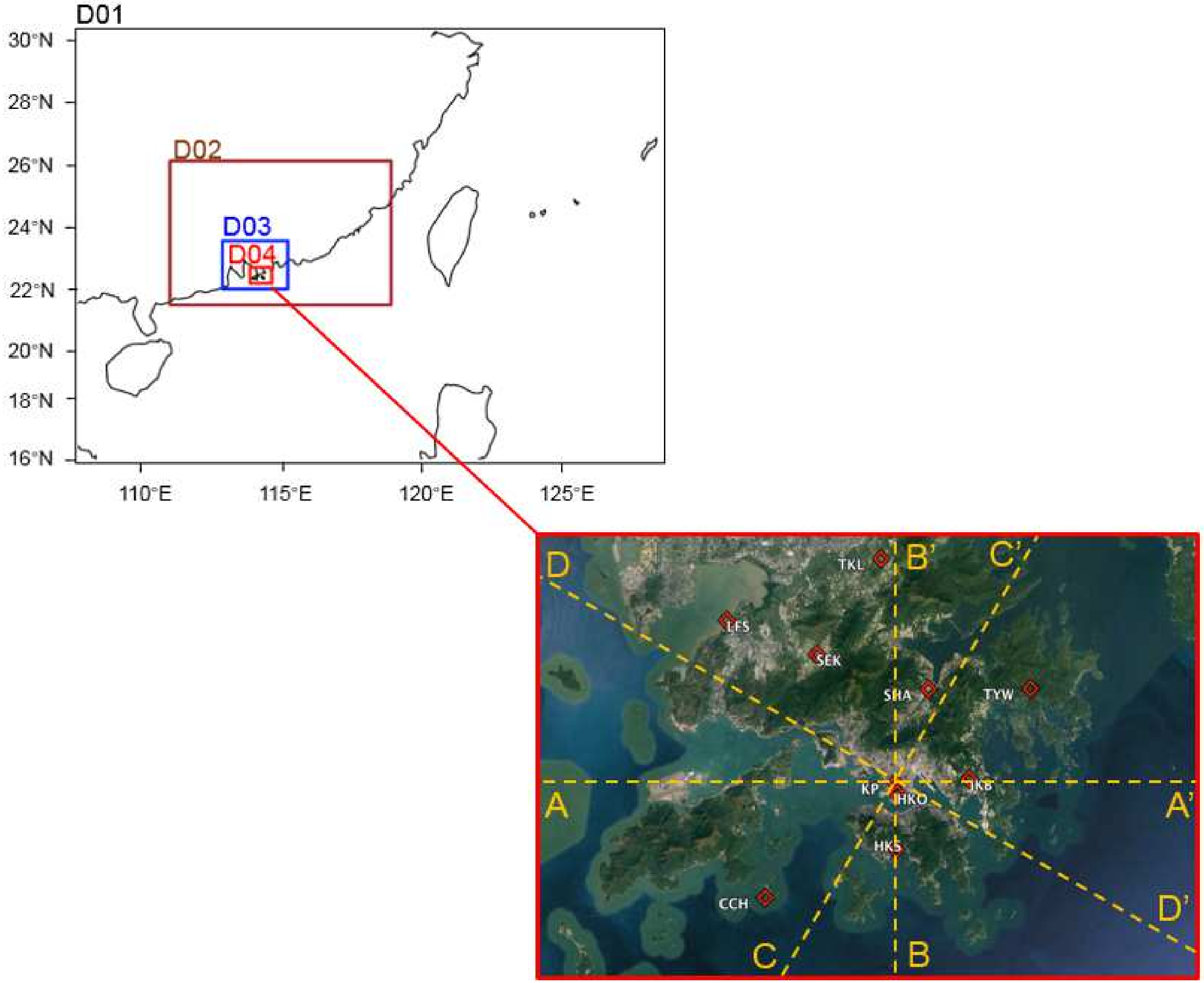

Figure 1. Computation domains and the 10 selected HK weather stations (red circles). Also shown are the transects A-A', B-B', C-C', and D-D'.

169

To test the ACLI during an extreme temperature event, we developed the LCZBC map (including 30 urban classes) over HK by overlaying the LCZ map (Figure 2) on the BC map. The BC information was extracted from the Land Utilization Map of Planning Department (PlanD) of HK Special Administrative Region (HKSAR) at 10-m resolution [34]. In each of the 10 urban LCZ types, the BC data are further categorized into three classes (commercial, residential, and non-building; Table S1) according to the dominant LULC at individual model grids (Figure 2).

The physical parameterization schemes adopted in this study are listed in Table 1. To capture city-scale AC load, the WRF model is coupled with the multi-layer BEP and BEM [25, 26]. The building characteristics and AC configurations are set according to the BCs regardless of urban morphology (Table S2). These parameters are obtained from government codes, guidelines, surveys, and studies in literature [12-16].

Table 1. Physical parameterization schemes used in the WRF model.

Physics Options	Schemes	References
Boundary Layer	BouLac	[42]
Microphysics	Single-Moment 3-class	[43]
Land Surface	Noah	[44]
Cumulus	Kain-Fritsch	[45]
Short Wave Radiation	Dudhia	[46]
Long Wave Radiation	Rapid Radiative Transfer Model	[47]
Surface Urban	BEP/BEM	[25, 26]

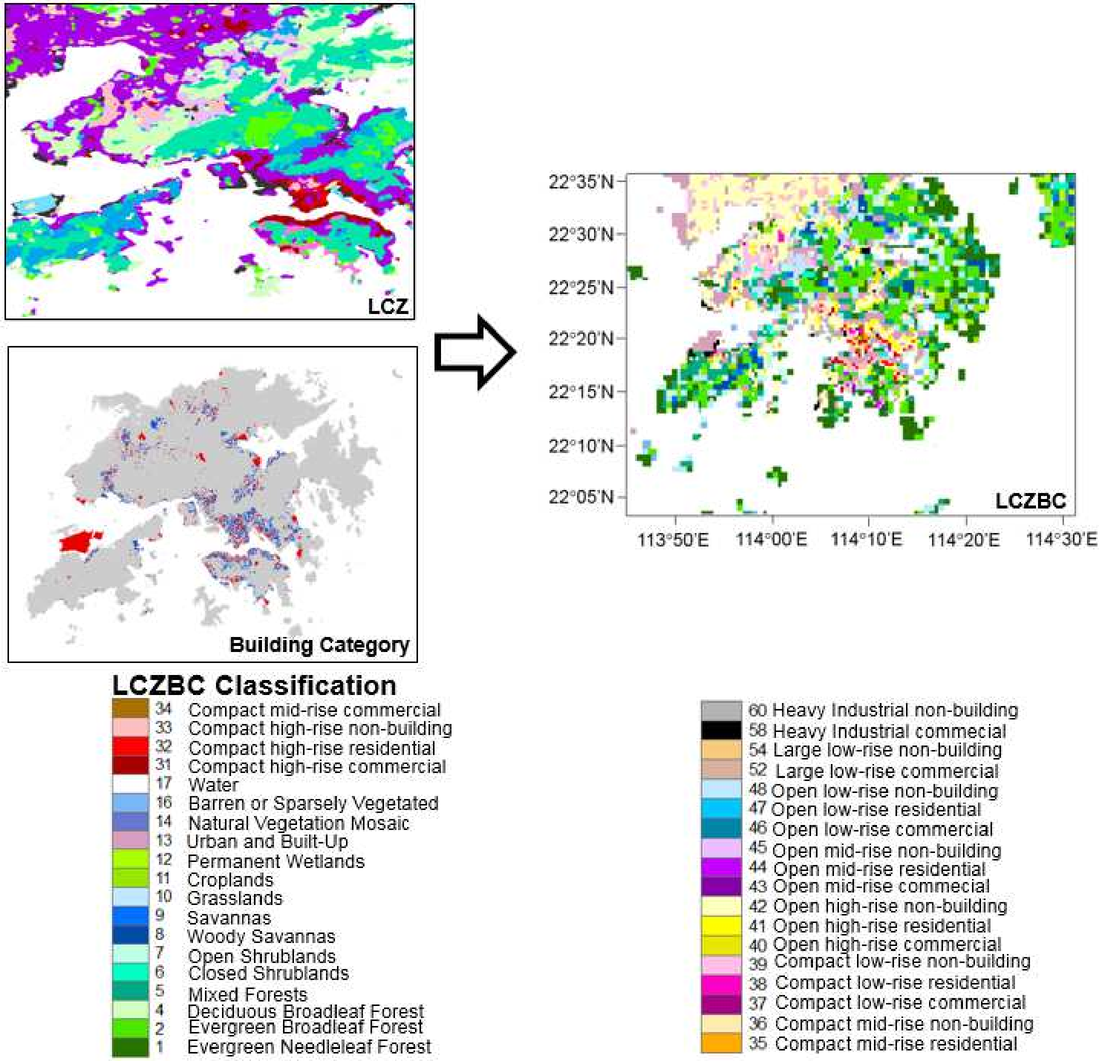

Figure 2. Development of the local climate zone and building category (LCZBC) map in Hong Kong.

2.2 Analytical Approach

2.2.1 Wind Information Layer

A schematic of summer wind information (Figure 3) was obtained from Urban Climatic Analysis Map of Hong Kong (UC-AnMap) [48] which was collectively developed based on observation, numerical simulation, and expert evaluation. UC-AnMap identified the summer (June to August) typical wind patterns. The prevailing southerly wind coincides with the summer background wind over HK during the analysis period [49]. In view of the prevailing wind, the southerly sea breeze could penetrate to North HK Island. Sea breeze was also observed along the Eastern and Western coastlines of Kowloon Peninsula. The Easterly channel wind establishes due to the narrow inlet to the East of Victoria Harbor, ventilating the downtown Kowloon Peninsula and the North central business district (CBD) on HK Island [7, 8]. Besides, the slope flows from Kowloon Peak or the hilly region on HK Island complicate the urban winds. UC-AnMap classifies the North HK Island and Kowloon Peninsula into 6 zones according to their dominant wind directions and urban ventilation characteristics [48].

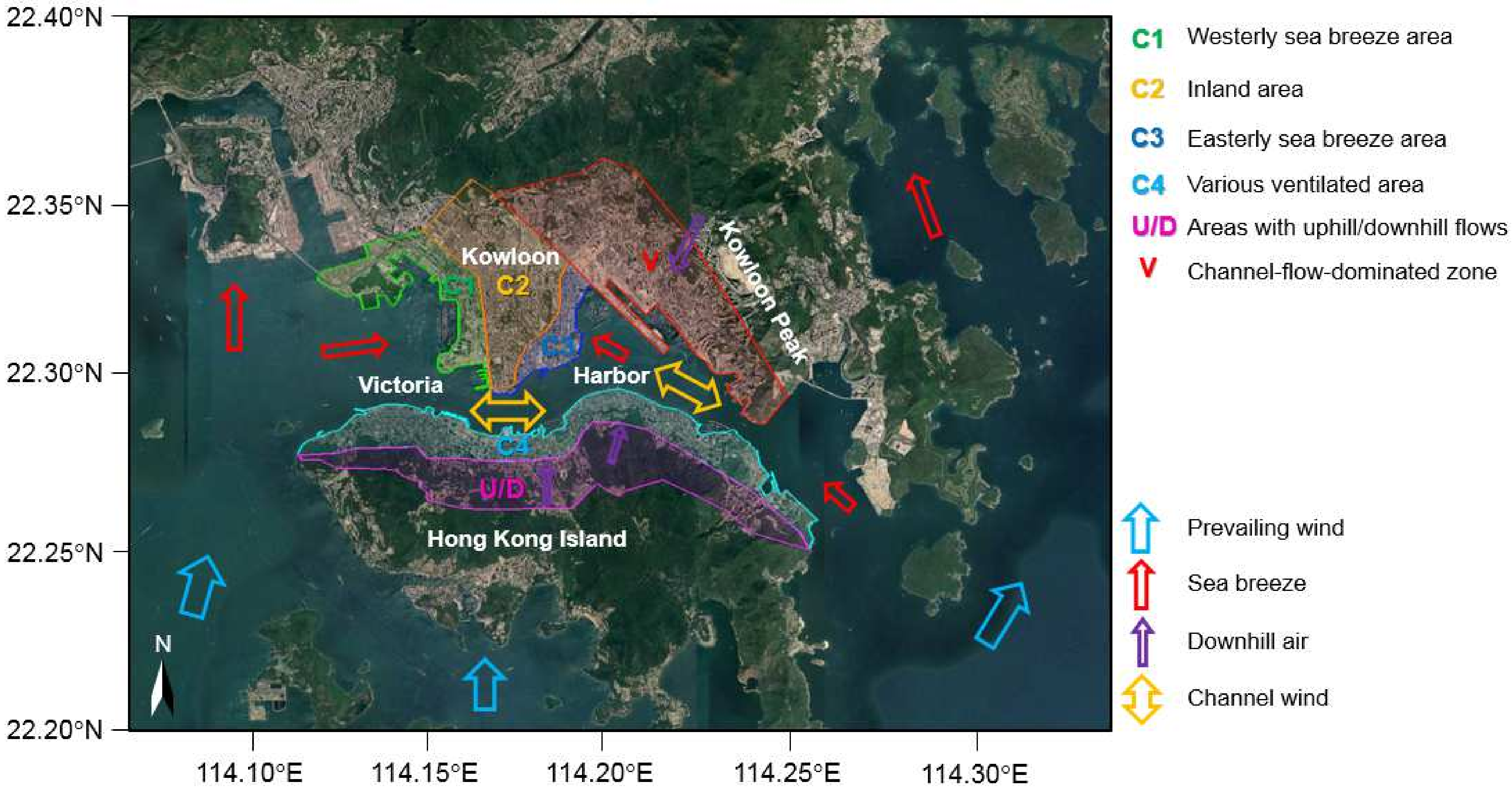

Figure 3. Wind information layer of Hong Kong in summer [48].

2.2.2 Numerical Experiment

To test the sensitivity of meteorology variables and AC load in downtown Kowloon (zone C2; Figure 3) to the surrounding mountains and urban areas, five numerical experiments, including one real scenario (REAL) and four hypothetical scenarios, are carried out (Table 2). The four hypothetical scenarios are: (1) a no-terrain scenario (ALLFlat) by removing all the terrain in (innermost) Domain 4 (Figure 1); (2) a no-urban scenario (ALLGreen) by switching all the urban areas in Domain 4 to grassland; (3) a scenario (NoV) by switching only the urban areas in Channel Wind Ventilation Zone V to grassland; and (4) a scenario (NoC4) by switching only the urban areas in Various Ventilation System Zone C4 to grassland (Figure 3).

2.3 Model Validation

The WRF model setup in this study had been fully validated in our previous study [31]. Its results are validated against the measurements from 10 selected HKO weather stations (Figure 1). The root-mean-square errors (RMSEs) are calculated to evaluate the model performances by 2-m air temperature (*T*2), 2-m relative humidity (*RH*2), and 10-m wind speed (*W*10; Table 3) [31]. The WRF results and HKO measurements agree well with each other. Their maximum RMSEs are 1.4 °C, 11.16%, and 1.41 m sec^{-1} for *T*2, *RH*2, and *W*10, respectively. The numerical result could accurately represent the weather condition and urban contexts in HK during the analysis period (June 23 to 27, 2016).

Table 2. Design of numerical experiments.

Scenario		Numerical experiment	Model setup
Real	1	REAL	WRF coupled to BEP/BEM with the combination of LCZ data and BC data (LCZBC) as the LULC configuration.
Hypothetical	2	ALLFlat	Same as REAL but all the terrains in Domain 4 is flattened.
	3	ALLGreen	Same as REAL but all the urban areas in Domain 4 are switched to grassland.
	4	NoV	Same as REAL but only the urban areas in Channel Wind Ventilation Zone (V; Figure 3) are switched to grassland.
	5	NoC4	Same as REAL but only the urban areas in upstream Various Ventilation System Zone (C4; Figure 3) are switched to grassland.

Table 3. Root-mean-square errors (RMSEs) between the predicted and observed 2-m temperature (*T*2), 2-m RH (*RH*2), and 10-m wind speed (*W*10) at the 10 selected weather stations operated by HKO [50].

Station	Classification	LCZ type	RMSEs		
			*W*10 (m sec^{-1})	*RH*2 (%)	*T*2 (°C)
HKO	urban	LCZ1	1.38	9.83	1.4
KP	urban	LCZ4	1.10	9.89	1.04
HKS	suburban	LCZ5	1.20	8.15	1.05
JKB	suburban	LCZ4	0.79	9.8	0.96
LFS	suburban	LCZ4	1.41	9.7	0.98
SEK	suburban	LCZC	1.07	11.16	1.02
SHA	suburban	LCZ6	1.18	7.09	0.91
CCH	rural	LCZA	1.06	9.02	1.25
TKL	rural	LCZ6	0.88	8.90	1.31
TYW	rural	LCZ4	/	8.42	1.30

3. Results and Discussion

In this section, the combined influence of complex terrain, UHI, and land-sea breezes on ground-level thermal circulation and temperatures are investigated. Besides, we assess the effects of terrain-induced channel winds on heat advection in urban areas. The sensitivity of ACLI to terrain, UHI, and local flows is tested as well.

3.1 Effect of Mountains

3.1.1 Blockage

To quantify the effects of mountainous topography [51] on UHII and ACLI, one sensitivity experiment (ALLFlat) is conducted by flattening all the terrains in Domain 4 (Figure 1). Figure 4 compares $T2$ and $W10$ of the cases REAL and ALLFlat in early morning (0800 LST), late morning (1100 LST), early afternoon (1400 LST), late afternoon (1700 LST), evening (2000 LST), and late evening (2300 LST). The main discrepancy of $T2$ between the two cases ($\Delta T2_{R\text{-}ALLFlat}$) appears from late morning (1100 LST) to early afternoon (1400 LST) when the incoming solar radiation is most intense. Mountainous topography induces several high-temperature zones (35 °C to 37 °C, circles in Figure 4) in REAL where $T2$ is about 1 °C to 2 °C hotter than other areas. Whereas, these hot spots are not observed in ALLFlat where $T2$ is spatially more uniform. These five high-temperature zones could be bisected into two categories according to their dissimilar mechanisms underlying extreme temperatures. The first type (red dashed circles in Figure 4) consists of the zones on the mountain leeward. They are poorly ventilated where cooling sea breeze seldom sweeps directly due to the mountain blockage. The poor ventilation could be caused by the heat trap in street canyons and the subsequent elevated ground-level temperature. The second type (black dashed circles in Figure 4) includes the inland foothill zones between urban leeward and mountain windward. The southerly sea breeze penetrates the urban areas then ends up with stagnation in these zones due to mountain blockage. The heat from the upstream urban areas accumulates, elevating $T2$. Previous studies based on pointwise observation in HK found that the summertime high-temperature in the second type of foothill areas is attributed to the warming effect of mountains [52]. Whereas, the current results show that heat advection and accumulation are the main reasons for the hotter $T2$.

Energy impact in response to hills is further tested by the difference in sensible cooling demand ($\Delta SCD_{R\text{-}ALLFlat}$) between the cases REAL and ALLFlat. Figure 5 shows $\Delta SCD_{\mathrm{R\text{-}ALLFlat}}$ in early afternoon (1400 LST) when terrain causes maximum $\Delta T2_{R\text{-}ALLFlat}$. Compared with the ALLFlat test, the mountainous topography in REAL also results in heavier ACLI in some of the zones (about 38 W m^{-2}, red and black circles in Figure 5). These zones almost coincide with the aforementioned high-temperature zones (Figures 4a and 5). Whereas, the mountain blockage increases the AC load in the foothill zones A, B, C, and E (Figures 4 and 5), while there is no noticeable change in zone D. These increases in AC load are mainly attributed to their compact, high-rise urban setting (LCZ1-C/R, Figure 2) with the following two characteristics: (1) high-intensity AC usage and the subsequent strengthened AH, and (2) aggravated heat trap due to the deep street canyons in HK. As a result, the AC load in zones A, B, C, and E is more sensitive to the weakened winds on the leeward side than those in the low-density urban or the non-building areas in zone D.

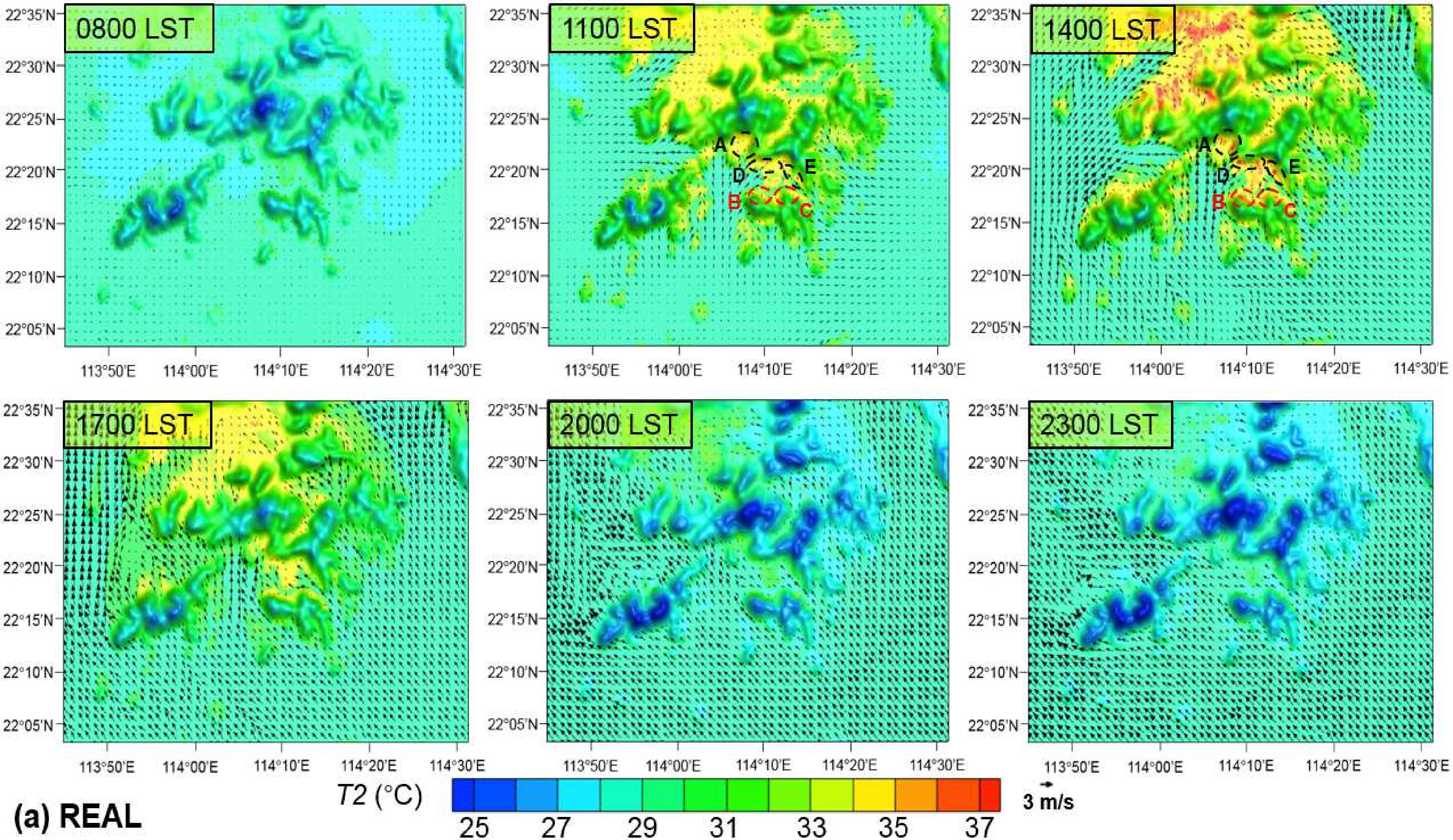
0800 LST
1100 LST
1400 LST
1700 LST
2000 LST
2300 LST
A
B
C
D
E
22°35'N
22°30'N
22°25'N
22°20'N
22°15'N
22°10'N
22°05'N
113°50'E
114°00'E
114°10'E
114°20'E
114°30'E
T2 (°C)
25
27
29
31
33
35
37
3 m/s
(a) REAL

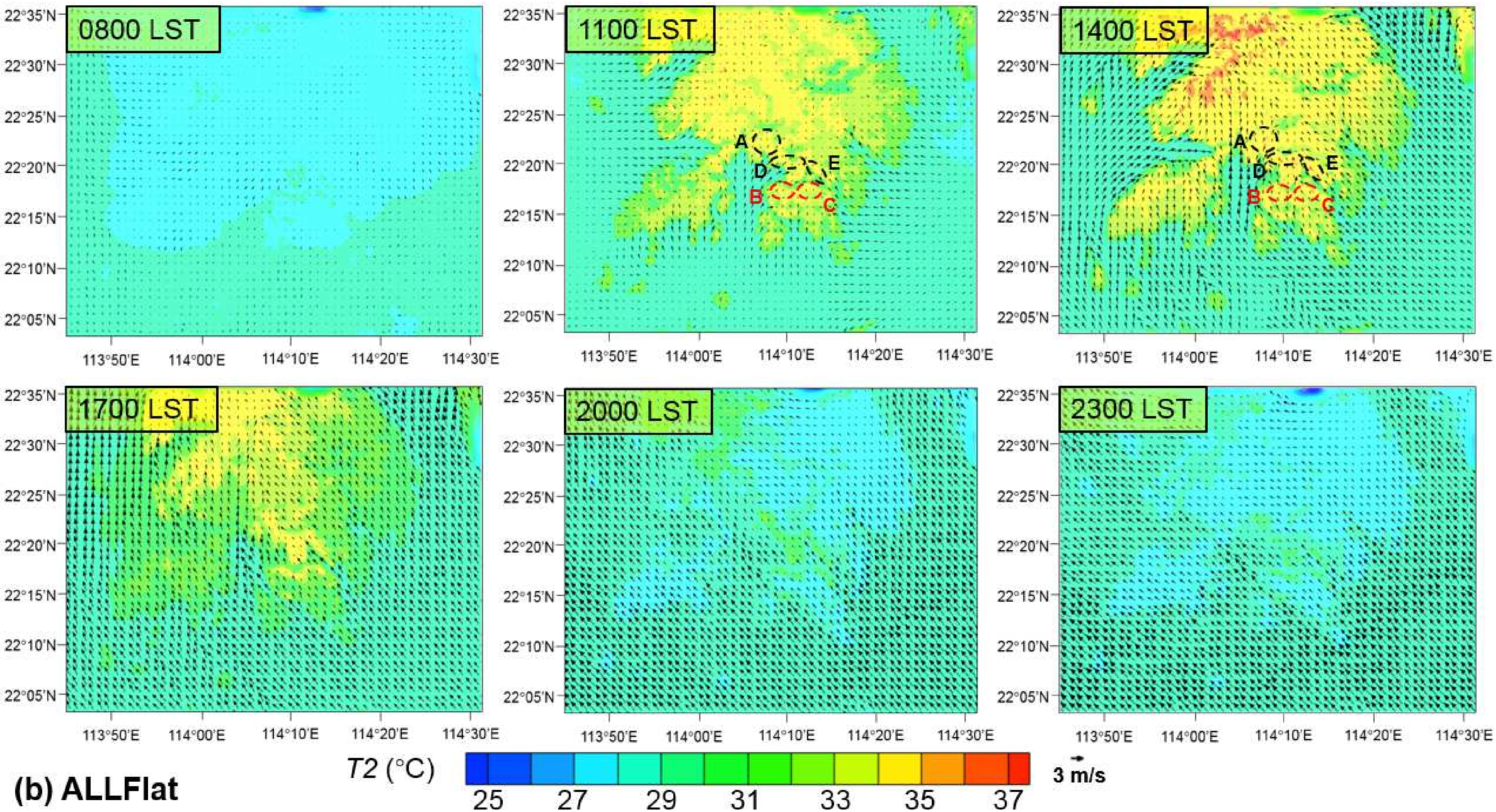

Figure 4. 2-m air temperatures ($T2$; shaded contours) and 10-m winds ($W10$; vectors) of the (a) REAL and (b) ALLFlat cases in early morning (0800 LST), late morning (1100 LST), early afternoon (1400 LST), late afternoon (1700 LST), evening (2000 LST), and late evening (2300 LST). The red and black circles (dashed lines) denote the foothill areas on the leeward and windward sides, respectively.

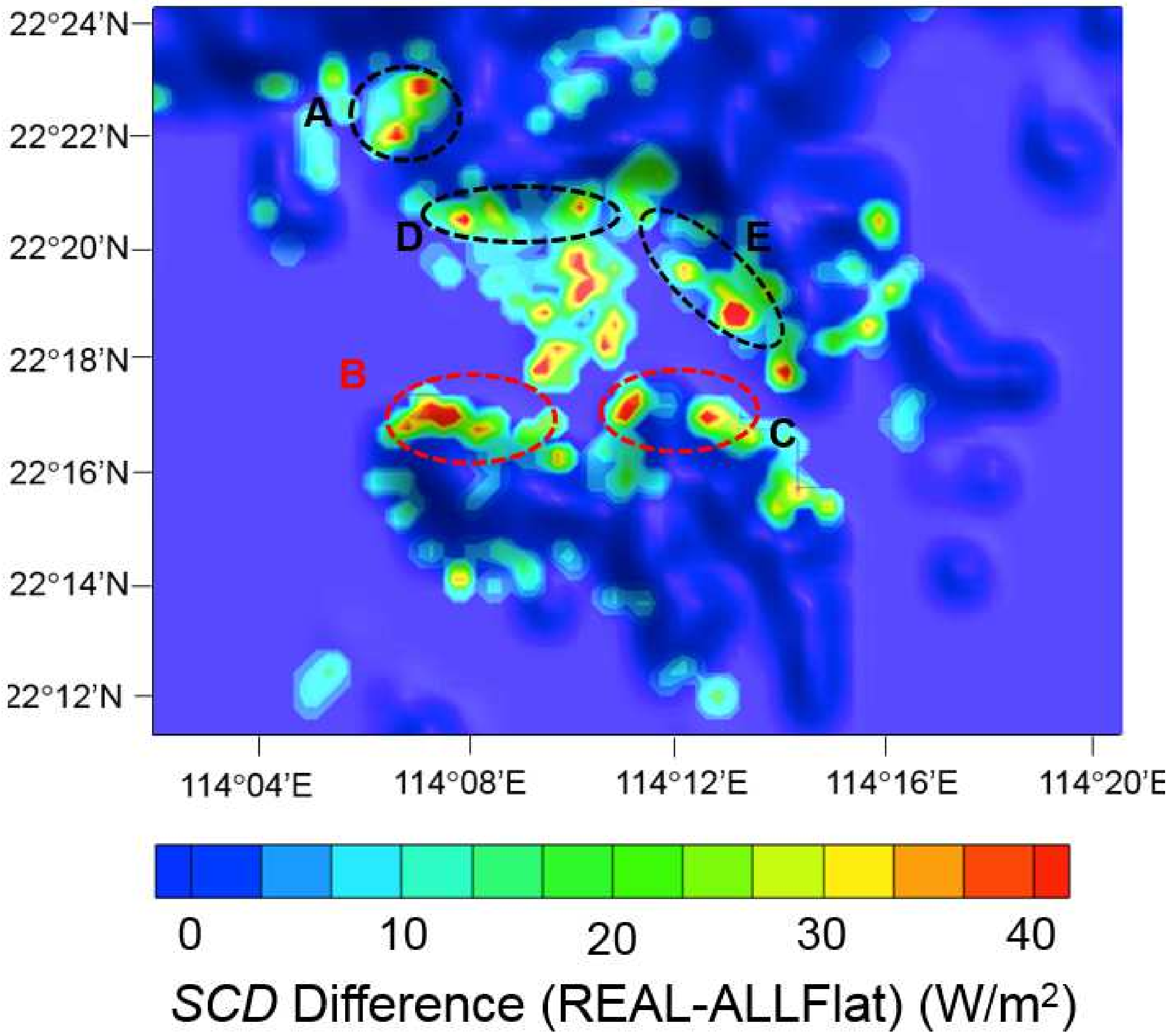

Figure 5. Difference in sensible cooling load between the cases REAL and ALLFlat $\Delta SCD_{R\text{-}ALLFlat}$ at 1400 LST. The red and black circles (dashed lines) denote the foothill areas on the leeward and windward sides, respectively.

3.1.2 Channeling

Although the channel winds in east Victoria Harbor have been reported elsewhere [7, 8, 48, 53], their development mechanism worth investigation. To test the sensitivity of channel winds to UHI, one numerical experiment (ALLGreen) is conducted by switching all the urban areas to grassland in the innermost Domain 4 (Figure 1). Figure 6 compares the U-component (easterly) wind velocity at 10-m (*U*10) and 50-m (*U*50) elevation in the channel winds between the REAL and ALLGreen cases. Compared with the REAL case, the maximum *U*10 (*U*50) of the ALLGreen case is 1.45 m sec^{-1} (1.66 m sec^{-1}) slower at the eastern (narrow) inlet of Victoria Harbor, suppressing the channel winds locally. The UHI in the ALLGreen test is switched off that in turn weakens the vertical (buoyant) flows and the thermal forcing for horizontal winds. Eventually, the sea breeze would escape from the eastern narrow inlet of Victoria Harbor, diverting to areas with lower resistance. In addition to rough terrains, this finding shows that downwind UHI could be important to channel-flow development under calm winds.

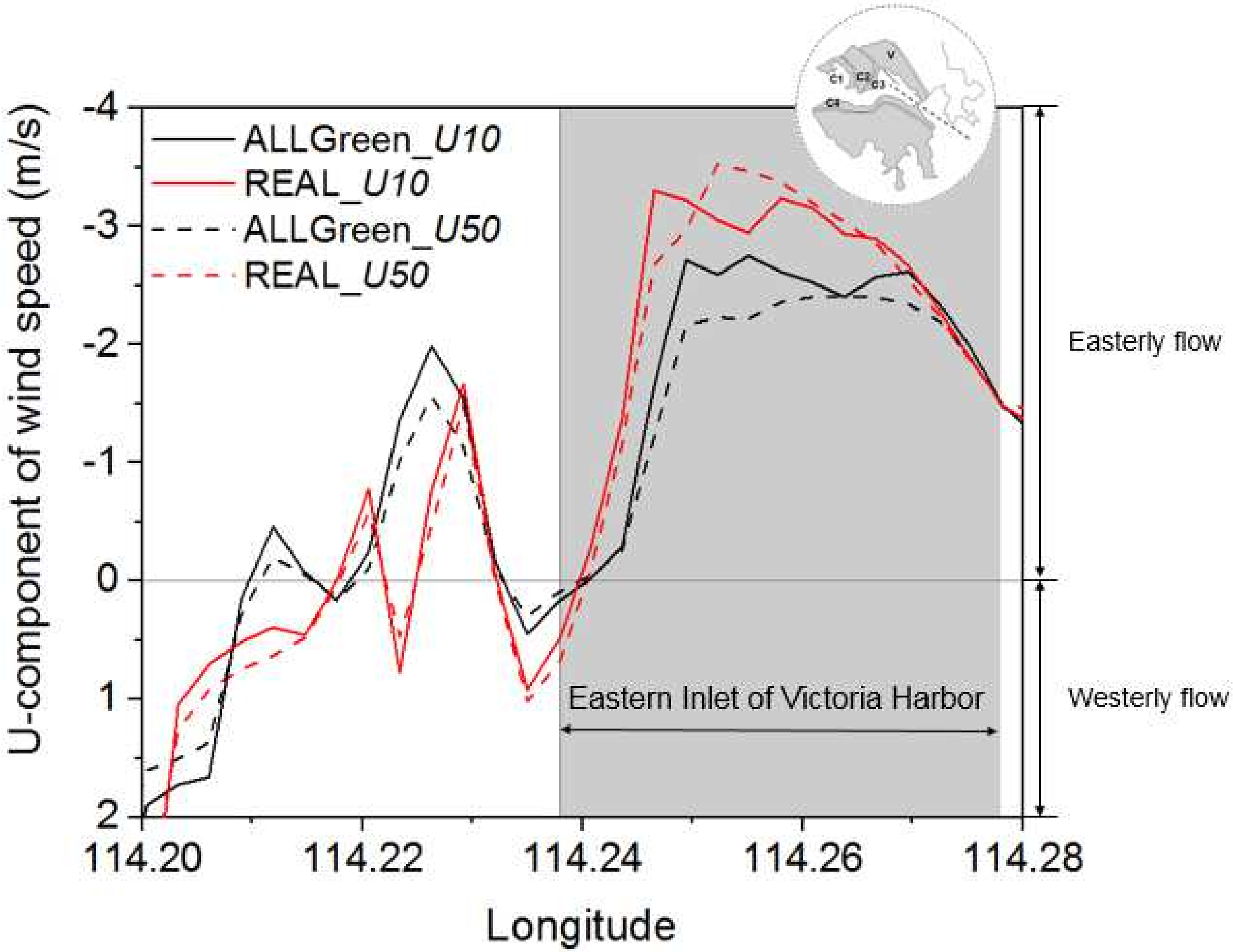

Figure 6. Comparison of the U-component wind velocity at 10-m (*U*10) and 50-m (*U*50) elevation on the vertical cross section along the channel wind (transect D-D’ in Figure 1 or the dashed line in the figure inserted) between the REAL and ALLGreen cases.

3.2 Heat Advection by Channeling

The hills (400 m to 550 m) on HK Island and Kowloon Peninsula flank Victoria Harbor that collectively initiate the (southeasterly) channel winds (Sections 2.2.1 and 3.1.2) [7, 8]. To test the sensitivity of heat advection to the channel winds, the meteorology parameters and ACLI under two characteristic wind patterns are compared (Figure 7). The first wind pattern develops from 0000 LST (midnight) on June 23, 2016 to 1400 LST (afternoon) on June 25, 2016 that consists of the westerly sea breeze and easterly channel flow (WSBECF) [54]. The ground-level winds $U10$ in each climate zone fluctuate between -1.71 m sec^{-1} (easterly wind) and 1.61 m sec^{-1} (westerly wind; Figure 7). The other wind pattern is characterized by stronger easterly channel flow (ECF, -2.59 m $sec^{-1} \leq U10 \leq$ -0.18 m sec^{-1}) from 1500 LST (afternoon) on June 25, 2016 to 0000 LST (midnight) on June 29, 2016 (Figure 7).

The urban zone V (Figure 3) was classified as channel-flow-ventilated areas by urban climatic map (Section 2.2.1) [48]. To quantify the channel-flow-induced heat advection, one numerical experiment (NoV; Table 2) is carried out by replacing all the urban areas in zone V by grassland. The differences in $T2$ between the cases REAL and NoV ($\Delta T2_{R\text{-}NoCV}$) are compared under the two aforementioned wind patterns (WSBECF and ECF). Figure 7 shows the diurnal variation of the spatially averaged $\Delta T2_{R\text{-}NoV}$ for downwind coastal areas (zone C1). Here, spatial average is the average of all model grids (elevation z = 2 m) in a specific climate zone. As zone C1 is not contiguous to zone V, $\Delta T2_{R\text{-}NoV}$ of zone C1 could be attributed to the heat advection from zone V being driven by the easterly channel winds. The heat advection in turn induces significantly $\Delta T2_{R\text{-}NoCV}$ in zone C1 in daytime ($\leq$ 0.7 °C) but not at nighttime ($\leq$

0.2 °C). All $\Delta T2_{R\text{-}NoCV}$ increases are coincident with strong easterly winds ($U10 < 0$ m sec^{-1}) in Kowloon Peninsula (zones C1 to 3). The maxima of $\Delta T2_{R\text{-}NoV}$ in ECF are 0.31 °C and 0.18 °C higher in daytime and at nighttime, respectively, than their WSBECF counterparts. There are two reasons leading to the dissimilarity between the two patterns (Figure 8): (1) the stronger easterly channel winds in ECF carries more heat from zone V to zone C1 than does the moderate winds in WSBECF; and (2) the convergence of westerly sea breeze and easterly channel winds in WSBECF ends up with a stagnation that in turn suppresses the heat advection from the east.

The spatial average of $\Delta SCD_{R\text{-}NoV}$ in zone C1 is calculated to examine the influence of channel-flow-induced heat advection on the ACLI (Figure 7). Apparently, it is aroused significantly in daytime but not at nighttime. Heat advection could soar the ACLI up to 2.62 W m^{-2}. Under the WSBECF regime, the heat flux from Zone V is relatively low, and there is considerable time lag (about an hour) between outdoor temperature and AC load due to the heat storage in massive building envelope. Afterward, under the ECF when the heat flux from Zone V is larger, $\Delta SCD_{R\text{-}NoV}$ responds instantaneously to the diurnal $\Delta T2_{R\text{-}NoV}$ variation (Figure 7).

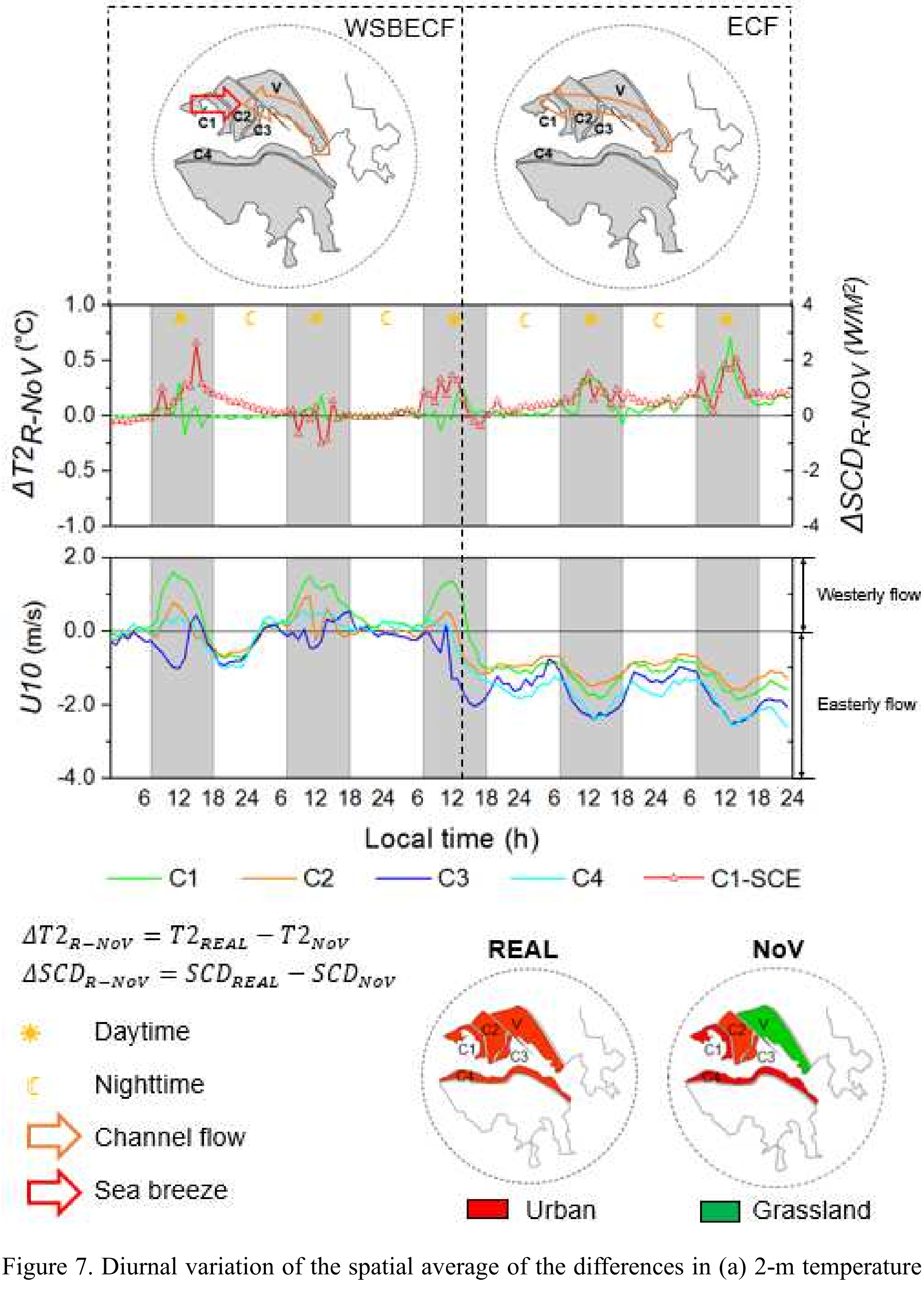

Figure 7. Diurnal variation of the spatial average of the differences in (a) 2-m temperature $\Delta T2_{R\text{-}NoV}$; (b) sensible cooling load $\Delta SCD_{R\text{-}NoV}$; and (c) 10-m U-component wind velocity $U10$ induced by Zone V urban areas for the flow patterns WSBECF and ECF.

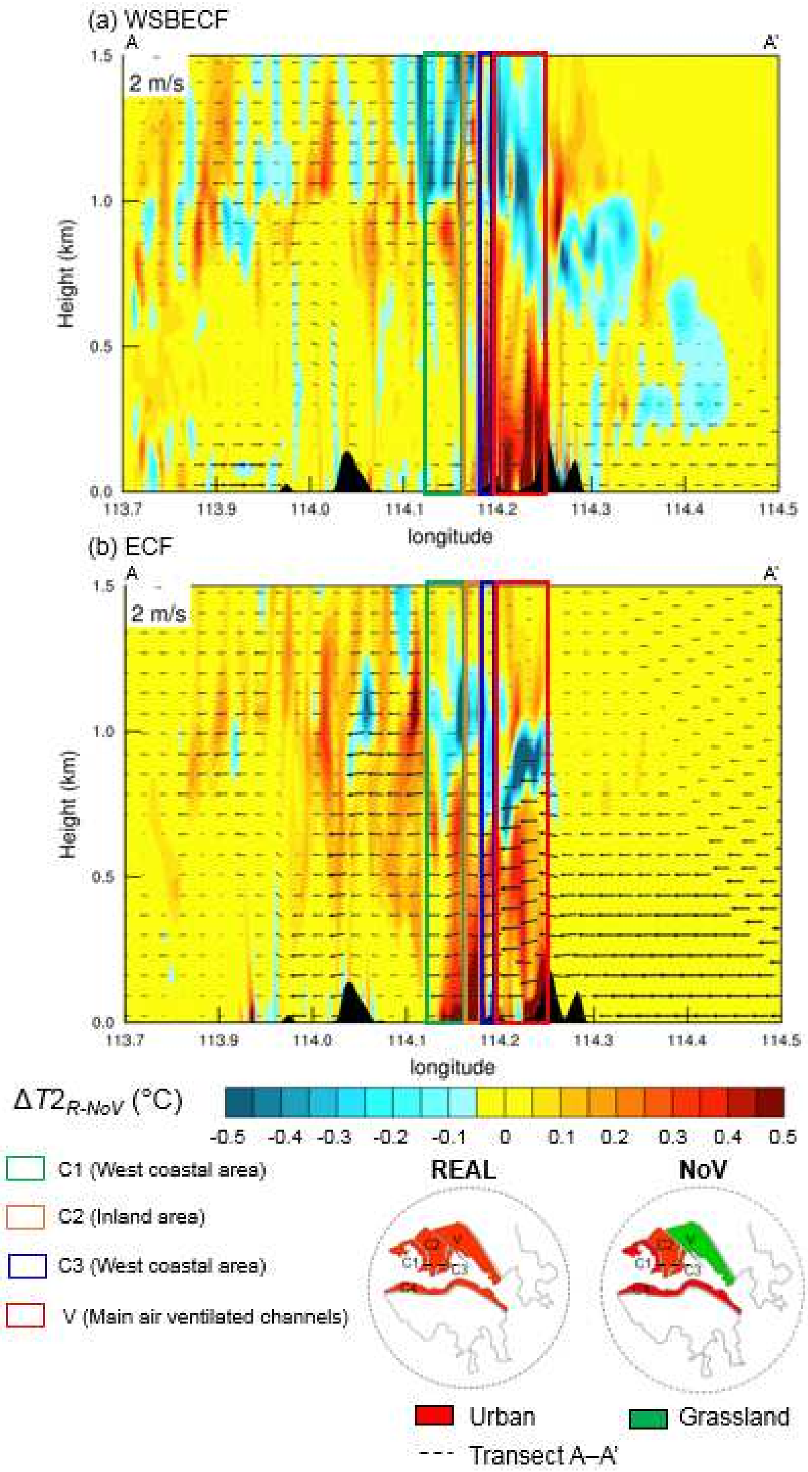

Figure 8. Vertical east-west cross section (transect A–A' in Figure 1) of the WRF-BEP/BEM model simulated wind velocity (m sec^{-1}; vectors) and the air temperature difference ($\Delta T_{R\text{-}NoV}$) between REAL scenario and scenario 4 (NoV) at 1400 LST for the flow patterns (a) WSBECF and (b) ECF.

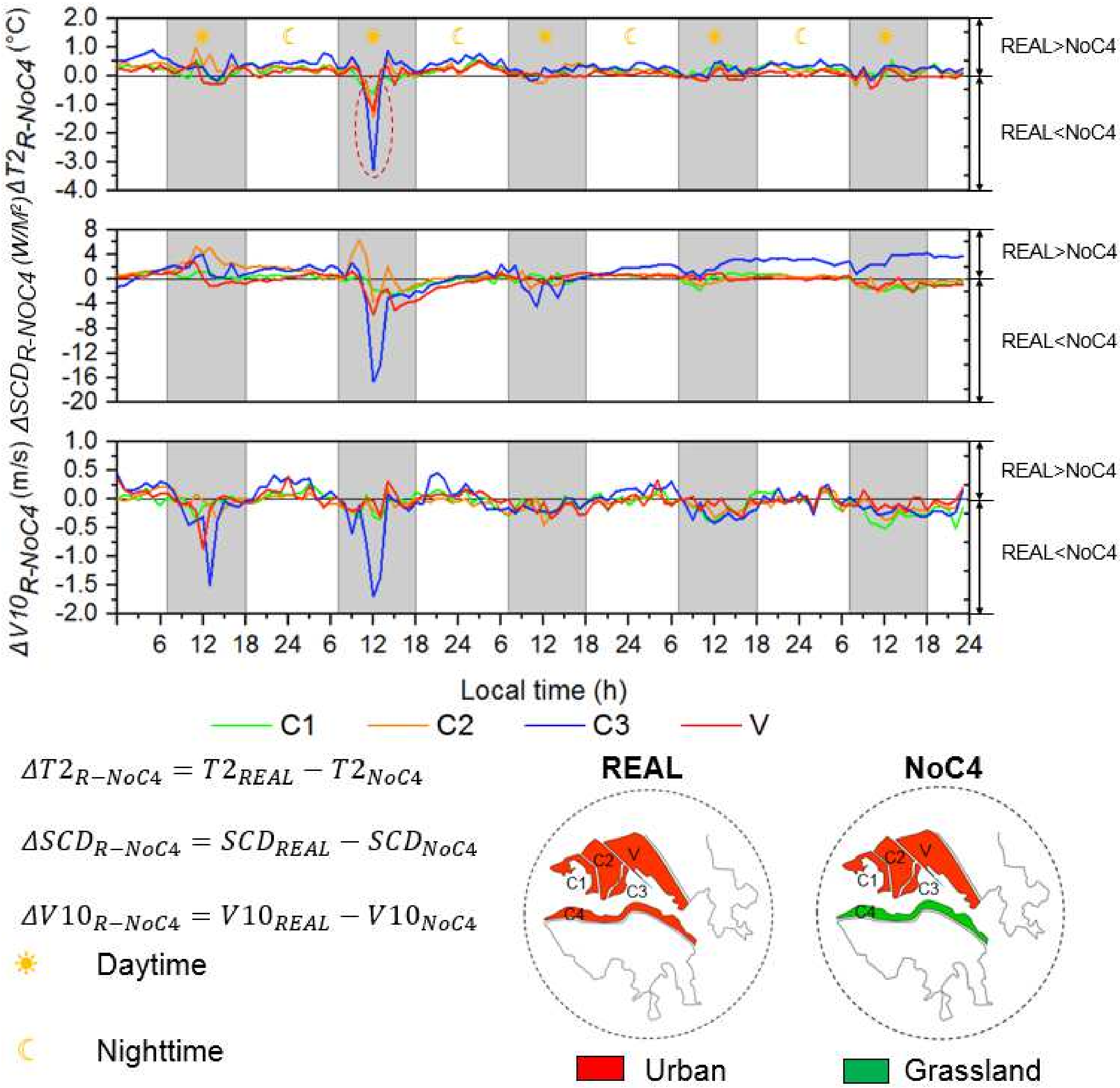

Figure 9. Diurnal variation of the spatial average of the differences in (a) 2-m temperature $\Delta T2_{R\text{-}NoC4}$; (b) sensible cooling load $\Delta SCD_{R\text{-}NoC4}$; and (c) 10-m V-component of wind velocity $V10$ induced by Zone C4 urban areas.

3.3 Urban-induced Local Wind

To test the sensitivity of urban climate to the surrounding urban-induced local flows, the changes in $T2$ ($\Delta T2_{R\text{-}NoC4}$) and $V10$ ($\Delta V10_{R\text{-}NoC4}$, V-component of wind velocity or southerly wind) between REAL and scenario 5 (NoC4; Table 2), are analyzed. In the NoC4 scenario, the UHI in the foothill C4 zone is switched off by replacing all the urban areas to grassland. The effect of C4-urban-induced local flows on the thermal environment of other zones (C1 to 3 and V) is investigated. Figure 9 compares the diurnal variation of the spatially averaged $\Delta T2_{R\text{-}NoC4}$ of C1 to 3 and V. The UHI in C4 tends to reduce $V10$ ($\Delta V10_{R\text{-}NoC4} < 0$ m sec^{-1}) and promote $T2$ ($\Delta T2_{R\text{-}NoC4} > 0$ °C) in daytime in other urban zones. $T2$ could increase by 0.9 °C while $V10$ could decrease beyond 0.86 m sec^{-1}. Compared with NoC4, the UHI in C4 zone in REAL induces a larger temperature difference between C4 zone and its surrounding vegetation/water surfaces (Figure 10). These temperature differences induce upslope flows [55] and urban-rural circulation over areas with uphill/downhill (U/D) winds and in C4 zones (marked in Figure 3), respectively, leading to characteristic local flows. Besides, the southerly (cooler) sea breeze developed under prevailing wind rises over the hills in HK Island that interacts with the local flows on the leeward side (right over C4). Eventually, it results in elevated turbulence levels (turbulence kinetic energy TKE ≈ 3 m^2 sec^{-2}) and stagnation locally. In contrast, in NoC4 scenario (Figure 10b), the southerly sea breeze no longer stagnates over C4 but penetrates farther inland to other urban zones (C1 to 3 and V). Subsequently, the penetrating sea breeze cools down the temperatures ($\Delta T2_{R\text{-}NoC4} > 0$ °C) that promotes the (northerly) wind speeds ($\Delta V10_{R\text{-}NoC4} < 0$ m sec^{-1}) in NoC4 than REAL. These findings indicate that the rugged terrains and foothill urban areas could couple upslope flows and urban-rural circulation. These local flows could further result in the convergence and stagnation of cooling sea breeze. In the worst scenario, ceasing the sea breeze would degrade the city ventilation, leading to UHI problems in the downwind areas.

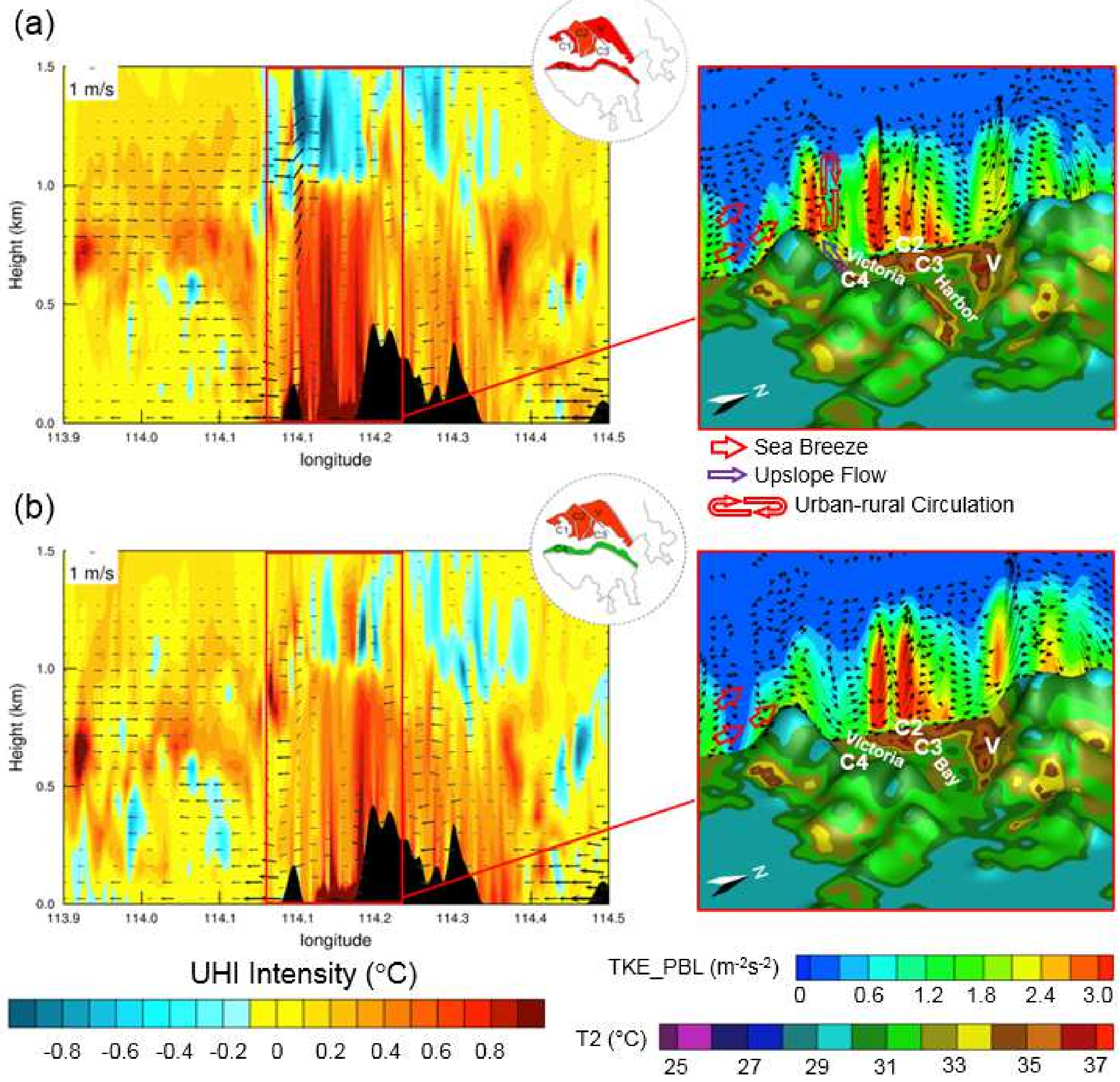

Figure 10. Vertical south-north cross section (transect C–C' in Figure 1) of the WRF-BEP/BEM model simulated velocity (m sec^{-1}; vectors), urban heat island UHI intensity (shaded contours on the left vertical planes), turbulence kinetic energy TKE (m^2 sec^{-2}; shaded contours on the right vertical planes), and the 2-m temperature *T*2 (shaded contours on the surface) at 1400 LST for (a) REAL scenario and (b) scenario 5 (NoC4).

The urban-induced upslope flows are only significant in daytime but not at nighttime. Figure 11 shows the *T*2 and V-component of ground-level wind speed (*GWS*) along a south-north transect (A-A' in Figure 1) at 1400 LST on June 25, 2016 when the temperature was peaked in the heatwave event (*T*2 = 35.5 °C) [40]. Here, *GWS* signifies the V-component of wind velocity at 50-m elevation where it was less affected by the buildings. In daytime, *GWS* in the REAL test drops sharply over Zone C4 that is 2.40 m sec^{-1} slower than its NoC4 counterpart over the downwind inland areas (C2). At nighttime, however, both tests have comparable *GWS* over Zone C2. The intense daytime solar radiation elevates the sensible heat flux over Zone C4. The thermally induced turbulence at the upper atmospheric boundary layer (about 1,000-m elevation; Figure 10) constrains the sea-breeze penetration. The hotter daytime *T*2 in Zone C2 in REAL is attributed to the poor ventilation. In contrast, the lower sensible heat flux at nighttime and the associated weaker vertical motion over Zone C4 impact insignificantly the sea-breeze penetration. The nocturnal $\Delta T2_{R\text{-}NoC4}$ (positive) could be attributed to the heat advection from Zone C4 to Zone C2.

On the other hand, the abrupt, negative $\Delta T2_{R\text{-}NoC4}$ (REAL< NoC4, red dashed circle in Figure 9) could be induced by the weakened easterly channel winds that in turn worsens the city ventilation. According to the ECF mechanism elaborated in Section 3.1.2, UHI plays an important role that is switched off hypothetically in NoC4. Hence, the (easterly) channel winds are not as strong as those in case REAL. As a result, poor ventilation dominates occasionally.

(a) Daytime

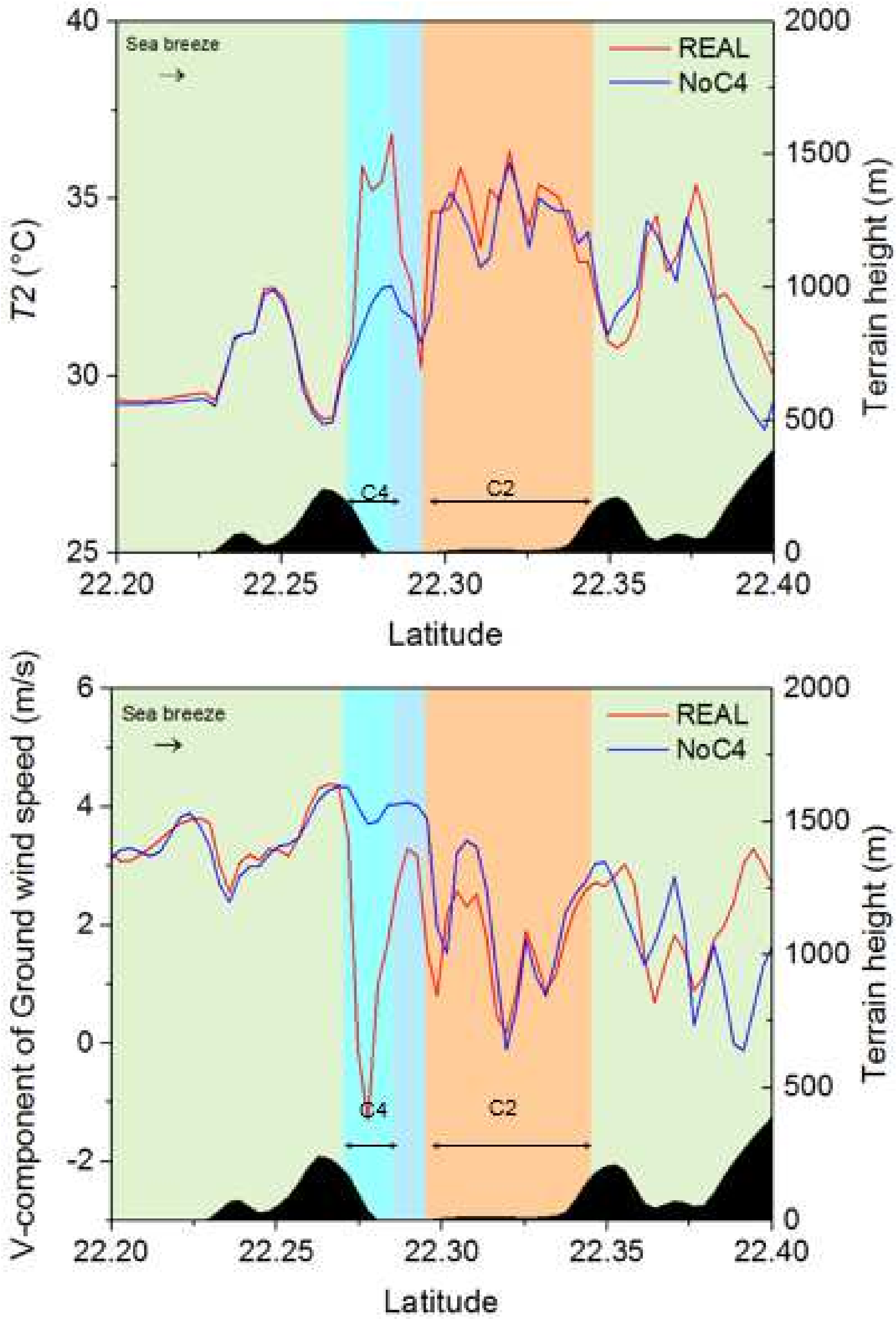

Sea breeze
REAL
NoC4
C4
C2
T2 (°C)
Terrain height (m)
Latitude
V-component of Ground wind speed (m/s)

(b) Nighttime

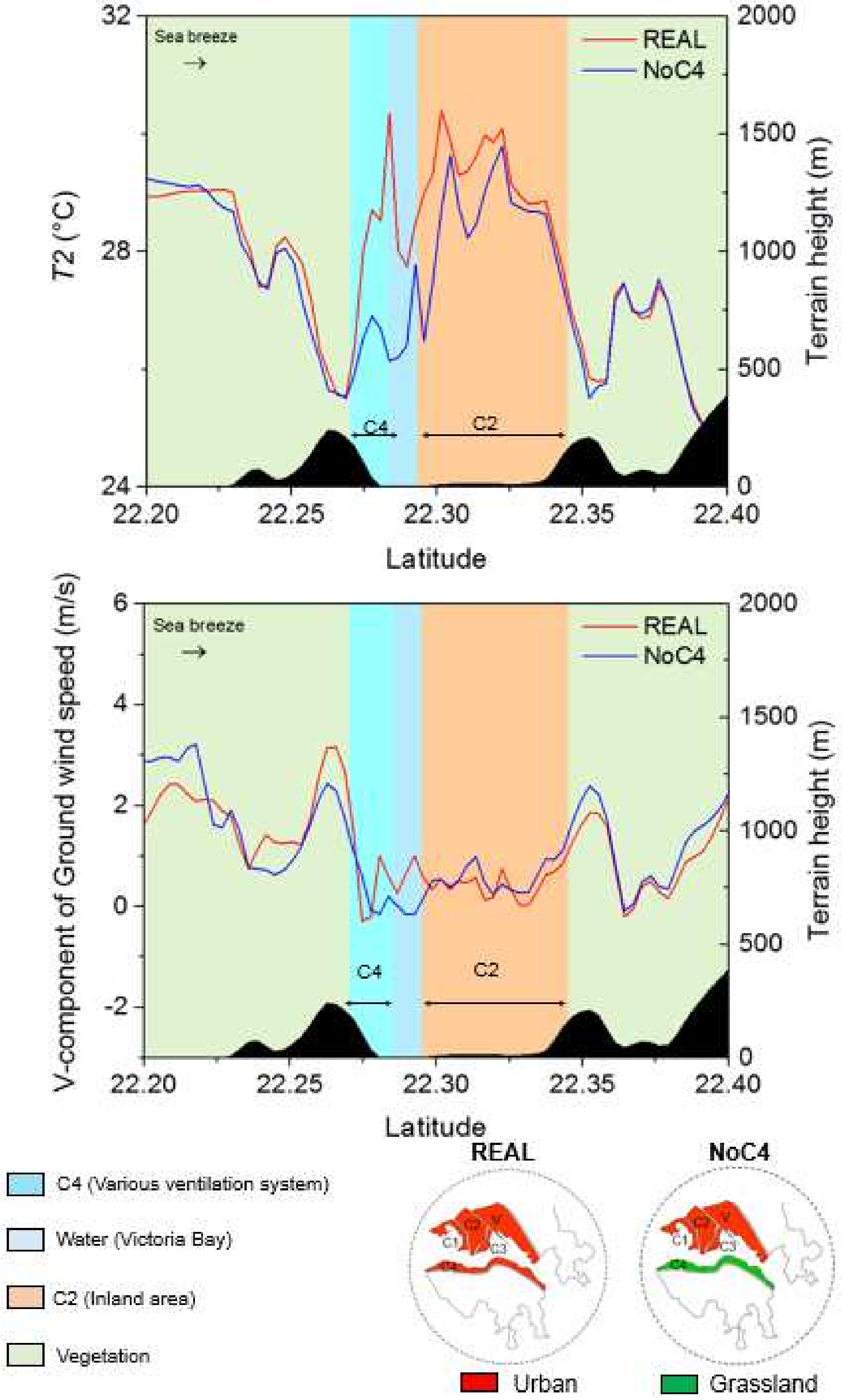

Figure 11. 2-m temperature *T*2, ground-level wind speed *GWS*, and terrain height along the transect B-B' at (a) 1400 LST and (b) 0400 LST on June 25, 2016.

Energy impact in response to local flows over Zone C4 is further tested by the difference in sensible cooling demand (ΔSCD_{R-NoC4}) between the cases REAL and NoC4 (Figure 9). Analogous to $\Delta T2_{R-NoC4}$, it is found that ΔSCD_{R-NoC4} is positive (REAL > NoC4) most of the time, while abrupt, negative ΔSCD_{R-NoC4} due to weakened easterly channel winds and infrequent poor ventilation. Upwind, urban-induced local flows would soar the ACLI as much as 6.41 W m^{-2} in the downwind urban areas. The diurnal variation of ΔSCD_{R-NoC4} is consistent with that of $\Delta T2_{R-NoC4}$. Whereas, there is delayed response of ΔSCD_{R-NoC4} to the change in $\Delta T2_{R-NoC4}$. It is mainly because of the time lag between outdoor temperatures and building energy consumption discussed previously (Section 3.2).

The synergistic warming effect of UHI, sea breeze, and mountainous terrain has been reported elsewhere. Alike this study, it was found that the winds are blocked by urban heating on the mountain leeward side using an idealized WRF model [56]. Whereas, our current findings offer more insight. First of all, we unveiled different representative wind patterns and the associated mechanism. In this paper, the UHI-mountain-induced stagnation of upstream sea breeze inhibits its cooling capability in downstream urban areas instead of resulting in foehn-like winds. Secondly, we emphasize the interaction of urban zones rather than consolidating them as a whole because upstream urban zones might stagnate the inland penetration of cooling sea breeze. Finally, our current results are based on real weather conditions that are extended to building energy consumption.

4. Conclusions

In this study, the maps of LCZ and building category (LCZBC) of HK are integrated into a multi-layer WRF-BEP/BEM model. It is then used to investigate the coupling among rough terrain, UHI, land-sea breeze, and the associated local winds in a coastal city. Furthermore, the sensitivity of inland urban temperature and AC load to the surrounding mountainous terrain and UHI during a heatwave event (June 23 to 28, 2016) in HK is tested. The key findings are summarized as follows:

1. Mountain blockage promotes the 2-m temperature $T2$ by 1 °C to 2 °C in the foothill areas (zones A-E; Figure 3). The increase in $T2$ is mainly attributed to two factors. The first factor is inhibited sea-breeze penetration by mountains which restrains the cooling effect offered by maritime winds. The second factor is wind stagnation and the subsequent heat accumulation induced by mountains downwind the urban areas. Mountainous terrain could also arouse ACLI (about 5 W m^{-2} higher). In compact, high-rise cities where the heat trap is reinforced, ACLI is more sensitive to the mountain-induced extreme temperatures.

2. Both downwind UHI and channeling effect of mountains could be essential to channel-flow development. Downwind UHI could accelerate the 10-m $U10$ and 50-m $U50$ wind speeds as much as 1.45 m sec^{-1} (54.32%) and 1.66 m sec^{-1} (50.26 %), respectively.

3. Channel winds would result in heat advection, elevating UHII (0.7 °C higher in daytime and 0.2 °C at nighttime) downwind the urban areas. The stronger channel winds are, the

higher the temperature increases. Moreover, horizontal flows, such as see breeze from the opposite direction, could suppress channel-flow-induced heat advection. Besides, heat advection could promote the ACLI as much as 2.62 W m^{-2}. Compared with weak channel-wind pattern, ACLI is more sensitive to heat advection that responds more quickly to outdoor temperatures in stronger channel winds. The time lag between temperature and ACLI is negligible if the channel wind speed is faster than 2 m sec^{-1}.

4. UHI in foothill areas would interact with mountains, resulting in upslope flows and UHI circulation. These local flows could stagnate cooling sea breeze, slow down the winds (as much as 0.8 m sec^{-1}), and increase the temperature (about 0.9 °C) in downwind inland areas. Urban-induced upslope flows are only significant in daytime but not at nighttime. Daytime solar radiation induces large sensible heat flux and intense turbulence on the leeward side of mountain, which in turn block sea-breeze penetration. Whereas, the local flows are too weak to affect sea-breeze incursion at nighttime. Moreover, upwind urban-induced local flows could raise the ACLI as much as 6.41 W m^{-2} in downwind urban areas.

In brief, we demonstrate the synergy of urban-heat-island circulation, coastal winds, local winds, and complex terrain on urban warming and building energy consumption. A few representative wind patterns were developed thereafter. Their physical significance and the mechanism behind are elaborated. These wind patterns could occur in other coastal cities surrounded by hilly terrain such as San Francisco, Vancouver, Beijing or Taipei. The current findings could provide useful references to researchers and partitioners.

Acknowledgments

This research is conducted in part using the research computing facilities and/or advisory services offered by Information Technology Services (ITS), The University of Hong Kong (HKU). Technical support from Ms. Lilian Y.L. Chan, Mr. W.K. Kwan, and Mr. Bill H.T. Yau is appreciated. This study is partly supported by the Hong Kong (HK) Research Grants Council (RGC) Theme-based Research Scheme (TRS)T24-504/17-N, the RGC Collaborative Research Fund (CRF) C7064-18G and RGC CRF C5108-20G as well as the RGC General Research Fund (GRF) 17209819 and 17211322. X-X Li acknowledges the support by Guangdong Basic and Applied Basic Research Foundation (Grant No. 2021A1515011890). The authors are very thankful for the constructive comments raised by the two anonymous reviewers. Their insightful reviews are detailed and helpful to improve the manuscript.

References

[1] IEA, The Future of Cooling in China, Delivering on action plans for sustainable air conditioning, (2019) https://www.iea.org/reports/the-future-of-cooling-in-china.

[2] IEA, The Future of Cooling, Opportunities for energy- efficient air conditioning, (2018) https://www.iea.org/reports/the-future-of-cooling.

[3] B. Stone Jr, E. Mallen, M. Rajput, C.J. Gronlund, A.M. Broadbent, E.S. Krayenhoff, G. Augenbroe, M.S. O'Neill, M. Georgescu, Compound Climate and Infrastructure Events: How Electrical Grid Failure Alters Heat Wave Risk, Environmental Science & Technology, 55 (10) (2021) 6957-6964.

[4] J. Katzfey, H. Schlünzen, P. Hoffmann, M. Thatcher, How an urban parameterization affects a high‐resolution global climate simulation, Quarterly Journal of the Royal Meteorological Society, 146 (733) (2020) 3808-3829.

[5] A.L. Hirsch, J.P. Evans, C. Thomas, B. Conroy, M.A. Hart, M. Lipson, W. Ertler, Resolving the influence of local flows on urban heat amplification during heatwaves, Environmental Research Letters, 16 (6) (2021) 064066.

[6] L. Leo, H. Fernando, S. Di Sabatino, Near-surface flow in complex terrain with coastal and urban influence, Environmental Fluid Mechanics, 15 (2) (2015) 349-372.

[7] H. Liu, J.C. Chan, An investigation of air-pollutant patterns under sea–land breezes during a severe air-pollution episode in Hong Kong, Atmospheric Environment, 36 (4) (2002) 591-601.

[8] H. Liu, J.C. Chan, Boundary layer dynamics associated with a severe air-pollution episode in Hong Kong, Atmospheric Environment, 36 (12) (2002) 2013-2025.

[9] R. Bassett, X.M. Cai, L. Chapman, C. Heaviside, J.E. Thornes, Methodology to separate urban from regional heat advection by use of the Weather Research and Forecasting mesoscale model, Quarterly Journal of the Royal Meteorological Society, 143 (705) (2017) 2016-2024.

[10] F.Y. Cheng, Y.T. Wang, M.Q. Huang, P.L. Lin, C.H. Lin, P.H. Lin, S.H. Wang, B.J. Tsuang, Boundary layer characteristics over complex terrain in central Taiwan: observations and numerical modeling, Journal of Geophysical Research: Atmospheres, 127 (2) (2022) e2021JD035726.

[11] F.N. Ribeiro, A.P. de Oliveira, J. Soares, R.M. de Miranda, M. Barlage, F. Chen, Effect of

sea breeze propagation on the urban boundary layer of the metropolitan region of Sao Paulo, Brazil, Atmospheric Research, 214 (2018) 174-188.

[12] J. Yang, Y. Wang, B. Xue, Y. Li, X. Xiao, J.C. Xia, B. He, Contribution of urban ventilation to the thermal environment and urban energy demand: Different climate background perspectives, Science of the Total Environment, 795 (2021) 148791.

[13] Y. Olivo, A. Hamidi, P. Ramamurthy, Spatiotemporal variability in building energy use in New York City, Energy, 141 (2017) 1393-1401.

[14] L. Frayssinet, L. Merlier, F. Kuznik, J.-L. Hubert, M. Milliez, J.-J. Roux, Modeling the heating and cooling energy demand of urban buildings at city scale, Renewable and Sustainable Energy Reviews, 81 (2018) 2318-2327.

[15] C.H.H. Wong, M. Cai, C. Ren, Y. Huang, C. Liao, S. Yin, Modelling building energy use at urban scale: A review on their account for the urban environment, Building and Environment, 205 (2021) 108235.

[16] R. Pokhrel, N.D. Ramírez-Beltran, J.E. González, On the assessment of alternatives for building cooling load reductions for a tropical coastal city, Energy and Buildings, 182 (2019) 131-143.

[17] F. Salata, S. Falasca, V. Ciancio, G. Curci, P. de Wilde, Climate-change related evolution of future building cooling energy demand in a Mediterranean Country, Energy and Buildings, 290 (2023) 113112.

[18] Y. Arima, R. Ooka, H. Kikumoto, T. Yamanaka, Effect of climate change on building cooling loads in Tokyo in the summers of the 2030s using dynamically downscaled GCM data, Energy and Buildings, 114 (2016) 123-129.

[19] F.B. Errebai, D. Strebel, J. Carmeliet, D. Derome, Impact of urban heat island on cooling energy demand for residential building in Montreal using meteorological simulations and weather station observations, Energy and Buildings, 273 (2022) 112410.

[20] Z. Jandaghian, U. Berardi, Analysis of the cooling effects of higher albedo surfaces during heat waves coupling the Weather Research and Forecasting model with building energy models, Energy and Buildings, 207 (2020) 109627.

[21] I. Adilkhanova, M. Santamouris, G.Y. Yun, Coupling urban climate modeling and city-scale building energy simulations with the statistical analysis: Climate and energy implications of high albedo materials in Seoul, Energy and Buildings, 290 (2023) 113092.

[22] L. Shen, H. Li, L. Guo, B.-J. He, Thermal and energy benefits of rooftop photovoltaic panels in a semi-arid city during an extreme heatwave event, Energy and Buildings, 275 (2022) 112490.

[23] S. Garshasbi, A. Khan, M. Santamouris, On the building cooling energy penalty of photovoltaic solar panels in Sydney, Energy and Buildings, (2023) 113259.

[24] H. Campanico, P.M. Soares, R.M. Cardoso, P. Hollmuller, Impact of climate change on building cooling potential of direct ventilation and evaporative cooling: A high resolution view for the Iberian Peninsula, Energy and Buildings, 192 (2019) 31-44.

[25] F. Salamanca, A. Krpo, A. Martilli, A. Clappier, A new building energy model coupled with an urban canopy parameterization for urban climate simulations—part I. formulation, verification, and sensitivity analysis of the model, Theoretical and applied climatology, 99 (3) (2010) 331-344.

[26] F. Salamanca, A. Martilli, A new building energy model coupled with an urban canopy parameterization for urban climate simulations—Part II. Validation with one dimension off-line simulations, Theoretical and Applied Climatology, 99 (3) (2010) 345-356.

[27] F. Salamanca, M. Georgescu, A. Mahalov, M. Moustaoui, M. Wang, B. Svoma, Assessing summertime urban air conditioning consumption in a semiarid environment, Environmental Research Letters, 8 (3) (2013) 034022.

[28] I.D. Stewart, T.R. Oke, Local climate zones for urban temperature studies, Bulletin of the American Meteorological Society, 93 (12) (2012) 1879-1900.

[29] C. Shu, A. Gaur, L.L. Wang, M. Bartko, A. Laouadi, L. Ji, M. Lacasse, Added value of convection permitting climate modelling in urban overheating assessments, Building and Environment, 207 (2022) 108415.

[30] K. Nakajima, Y. Takane, Y. Kikegawa, K. Yamaguchi, Improvement of WRF–CM–BEM and its application to high-resolution hindcasting of summertime urban electricity consumption, Energy and Buildings, 296 (2023) 113336.

[31] R. Du, C.-H. Liu, X.-X. Li, C.-Y. Lin, Effect of local climate zone (LCZ) and building category (BC) classification on the simulation of urban climate and air-conditioning load in Hong Kong, Energy, 271 (2023) 127004.

[32] HKCSD, Population Estimates, (2021) https://www.censtatd.gov.hk/en/scode150.html.

[33] D. Hinrichsen, Coastal waters of the world: trends, threats, and strategies, Island Press, 1999.

[34] UNFPA, The state of world population, Chapter 5 (Urbanization and sustainability in the 21st Century). (2013) http://www.unfpa.org/swp/2007/english/chapter_5/.

[35] L. Shi, Z. Luo, W. Matthews, Z. Wang, Y. Li, J. Liu, Impacts of urban microclimate on summertime sensible and latent energy demand for cooling in residential buildings of Hong Kong, Energy, 189 (2019) 116208.

[36] C. Lou, H. Yang, Y. Li, N.h. and Cheung, Energy audit of buildings: a case study of a commercial building in Causeway Bay of Hong Kong, HV&AC, 2006 (36-5) (2006) 44-50.

[37] CLP, CLP Power Launches Smart Power Consumption Plan to Support Hong Kong's Transformation into a Smart City, (2017) https://www.clpgroup.com/content/dam/clp-group/channels/media/document/2017/20170615_tc.pdf.coredownload.pdf.

[38] R. Du, J. Song, X. Huang, Q. Wang, C. Zhang, O. Brousse, P.W. Chan, High-resolution regional modeling of urban moisture island: Mechanism and implications on thermal comfort, Building and Environment, (2021) 108542.

[39] L.G.R. Santos, V.K. Singh, M.O. Mughal, I. Nevat, L.K. Norford, J.A. Fonseca, Estimating building's anthropogenic heat: a joint local climate zone and land use classification method, in: eSIM Conference 2021, 2020.

[40] HKO, The Weather of June 2016 https://www.hko.gov.hk/en/wxinfo/pastwx/mws2016/mws201606.htm, (2016) https://www.hko.gov.hk/en/wxinfo/pastwx/mws2016/mws201606.htm.

[41] Y. Wang, Y. Li, S. Di Sabatino, A. Martilli, P. Chan, Effects of anthropogenic heat due to air-conditioning systems on an extreme high temperature event in Hong Kong, Environmental Research Letters, 13 (3) (2018) 034015.

[42] P. Bougeault, P. Lacarrere, Parameterization of orography-induced turbulence in a

mesobeta--scale model, Monthly weather review, 117 (8) (1989) 1872-1890.

[43] S.-Y. Hong, J. Dudhia, S.-H. Chen, A revised approach to ice microphysical processes for the bulk parameterization of clouds and precipitation, Monthly weather review, 132 (1) (2004) 103-120.

[44] F. Chen, J. Dudhia, Coupling an advanced land surface–hydrology model with the Penn State–NCAR MM5 modeling system. Part I: Model implementation and sensitivity, Monthly weather review, 129 (4) (2001) 569-585.

[45] J.S. Kain, J.M. Fritsch, A one-dimensional entraining/detraining plume model and its application in convective parameterization, Journal of Atmospheric Sciences, 47 (23) (1990) 2784-2802.

[46] J. Dudhia, Numerical study of convection observed during the winter monsoon experiment using a mesoscale two-dimensional model, Journal of Atmospheric Sciences, 46 (20) (1989) 3077-3107.

[47] E.J. Mlawer, S.J. Taubman, P.D. Brown, M.J. Iacono, S.A. Clough, Radiative transfer for inhomogeneous atmospheres: RRTM, a validated correlated‐k model for the longwave, Journal of Geophysical Research: Atmospheres, 102 (D14) (1997) 16663-16682.

[48] HKPlanD, Urban climatic map and standards for wind environment - Feasibility Study., (2012).

[49] Y.Y. Yan, Surface wind characteristics and variability in Hong Kong, Weather, 62 (11) (2007) 312-316.

[50] HKO, Information of Weather Station, (2022) https://www.hko.gov.hk/en/cis/stn.htm.

[51] J.-F. Miao, L. Kroon, J. Vilà-Guerau de Arellano, A. Holtslag, Impacts of topography and

land degradation on the sea breeze over eastern Spain, Meteorology and Atmospheric Physics, 84 (3) (2003) 157-170.

[52] C. Zhang, Q. Wang, P.W. Chan, C. Ren, Y. Li, The effect of background wind on summertime daily maximum air temperature in Kowloon, Hong Kong, Building and Environment, 210 (2022) 108693.

[53] S.H. Yim, J.C. Fung, A.K. Lau, S.C. Kot, Developing a high‐resolution wind map for a complex terrain with a coupled MM5/CALMET system, Journal of Geophysical Research: Atmospheres, 112 (D5) (2007).

[54] Y. Wang, S. Di Sabatino, A. Martilli, Y. Li, M. Wong, E. Gutiérrez, P. Chan, Impact of land surface heterogeneity on urban heat island circulation and sea‐land breeze circulation in Hong Kong, Journal of Geophysical Research: Atmospheres, 122 (8) (2017) 4332-4352.

[55] L. Yang, Y. Li, City ventilation of Hong Kong at no-wind conditions, Atmospheric Environment, 43 (19) (2009) 3111-3121.

[56] C. Zhang, Q. Wang, P.W. Chan, Y. Li, Potential “downstream blocking” synergistic mechanism for urban warming in Kowloon Peninsula, Hong Kong, Urban Climate, 49 (2023) 101517.